Continuum Wind Flow Model: Introduction to Model Theory and Case Study Review

by

Elizabeth Walls

Continuum Wind Flow Model: Introduction to Model Theory and Case Study Review

Elizabeth Walls

Cancalia Engineering & Consulting, LLC, 101 Broadway, Oakland, CA, USA 94607
January 19, 2015 E-mail: liz@cancalia.com

ABSTRACT

When developing a wind farm, it is very important to accurately define the wind resource distribution across the project area such that an optimized turbine layout can be achieved. To estimate the wind resource distribution, typically, meteorological (met) towers are installed at various strategic locations and the wind speed and direction measured at these sites are used as inputs into wind flow models. Currently, linear and CFD models are most commonly used. Linear models can provide estimates quickly, with little training and at a low cost however, this type of model is well-known to deliver highly inaccurate estimates particularly in complex terrain. CFD models can provide more accurate estimates however they require significant computational time, an expert knowledge level and a much larger financial investment. Also, all commercially-available linear and CFD models are limited to using a single met site in the model creation.

A new wind flow model, Continuum (patent pending), is introduced which is based on a simplified analysis of Navier-Stokes and utilizes data from all of the met sites simultaneously to develop site-calibrated models. The model coefficients, m_{UW} and m_{DW}, describe the sensitivity of the wind speed to changes in the upwind and downwind terrain exposure and are defined for downhill and uphill flow. The coefficients are a function of terrain complexity and, since terrain complexity can change across an area, the estimates are performed in a stepwise fashion where a path of nodes with a gradual change in complexity are found between each pair of sites. Also, coefficients are defined for each wind direction sector and estimates are performed on a sectorwise basis. The site-calibrated models are created by cross-predicting between each pair of met sites and, through a self-learning technique, the model coefficients that yield the minimum met cross-prediction error are found.

A case study is presented where eleven met masts at a complex terrain site were modeled in Continuum. Using the site-calibrated model, the wind speeds were predicted at the met sites and excellent agreement was found between the estimated and actual wind speeds with a correlation coefficient of 0.96 and a RMSE of 0.90%. The largest wind speed estimate error was 1.6% and five of the eleven sites were modeled to within an error of 0.5%. In Continuum, a Round Robin analysis was performed using met subset sizes of 8, 9 and 10 mets where every possible combination of met sites were used to form a model which were then used to predict at the excluded met sites. The RMS error of the Round Robin predictions was ~1.6% for all three subset sizes which confirmed the very good quality, high level of robustness and validity of the Continuum wind flow model.

1. INTRODUCTION

In wind resource assessment, it is the primary goal to estimate the annual net energy that could be produced from a potential wind farm and this assessment includes several elements such as the wake loss model, the long-term climatic adjustments and, arguably the most important, the wind flow model [10, 15]. The wind flow model is the foundation of the wind resource assessment as it is used to estimate the free-stream (unwaked) wind speed distribution across the project area which is then converted into gross annual energy production. If the wind flow model is flawed or biased then all subsequent calculations will inherit those errors and the assessment will not be representative of the wind farm's true potential. It is therefore very important to have a robust wind flow model upon which to build the resource assessment.

The wind flow models that are currently most commonly used include linear models and computational fluid dynamics (CFD) models. In general, linear models are viewed as simple and quick to produce estimates but are known to produce estimates with significant error particularly in complex terrain [1–7, 11, 13, 16]. On the other end of the spectrum, CFD models are considered to be more robust and can produce estimates with fairly low error [6, 13, 16] however they are very expensive, both computationally and financially, and require an expert knowledge level in CFD to confidently produce a model [6, 13].

A new wind flow model named "Continuum" (patent pending) is introduced which can be viewed as the middle ground between linear and CFD models. The physics underlying Continuum tie back to the theory of conservation of momentum (Navier-Stokes) and, by making simplifying assumptions regarding the uniformity of the wind conditions, Continuum estimates the wind speed from one site to another based solely on how the terrain changes between the sites. In this paper, a brief introduction of Continuum and an overview of existing wind flow models are given first and, following this, the equations used in Continuum to predict the wind speed are derived from Navier-Stokes. Then, a case study which demonstrates the application of the Continuum wind flow model at a project with eleven met sites is presented and the wind speed estimate errors are examined.

2. CONTINUUM MODEL OVERVIEW

Continuum is a wind flow model that utilizes all available meteorological (met) sites simultaneously to generate site-calibrated terrain exposure models. The Continuum model describes the sensitivity of the wind speed to changes in the upwind (UW) and downwind (DW) terrain exposure by using two coefficients, m_{UW} and m_{DW}. The UW coefficient, m_{UW}, represents the sensitivity of the wind speed to changes in the UW exposure while the DW coefficient, m_{DW}, describes how the wind speed changes as the DW exposure varies.

Three sets of model coefficients are defined in Continuum which represent downhill flow, uphill flow and induced speed-up over hills. The coefficients are dependent on the level of terrain complexity and log-log relationships are used to describe the coefficients as a function of terrain complexity. Also, model coefficients are defined for each wind direction sector.

In Continuum, first, the default model coefficients are used to cross-predict the met site wind speeds and the overall cross-prediction error is determined by comparing the wind speed estimates with the measured values. Then, using a self-learning algorithm, the coefficient relationships are systematically altered and the relationships that yield the minimum met cross-prediction RMS error are found and these define the site-calibrated model.

The terrain exposure is calculated using four different radii of investigation (4000, 6000, 8000 and 10,000 m) and a site-calibrated model is formed for each radius. These models are then used to form estimates of the wind speed and gross annual energy production (AEP) at the turbine sites and/or at map nodes.

Since the model coefficients vary as a function of terrain complexity, the predictions between sites are conducted in a stepwise fashion where the wind speed is estimated along a path of nodes that have a gradual change in terrain complexity from one node to the next. In Continuum, between each pair of met sites and from each met site to every turbine site or map node, a path of nodes is created where there is a small change in the exposure and elevation from one node to the next. For each step along the path of nodes, the sectorwise UW and DW model coefficients are determined from the site-calibrated relationships based on the terrain complexity and whether the flow is downhill or uphill. The change in wind speed is then estimated along the path of nodes as the UW and DW exposure changes from the met site to the turbine or map node.

Wind speed and gross energy estimates are formed at the turbine or map node using each met site and each site-calibrated model. Then, based on the similarity of the UW and DW exposure between the predictor met and the target site, wind speed weights are assigned to each estimate. Additionally, the RMS of the met cross-prediction error is found for each site-calibrated model and the RMS error is used as a weight. The final estimate at the turbine or map node is therefore a weighted average of all estimates formed from each met site weighted by the terrain similarity and the RMS cross-prediction error of the site-calibrated models.

3. REVIEW/SUMMARY OF CURRENT STATE-OF-THE-ART WIND FLOW MODELS

Currently, there are two main types of wind flow models used in the wind industry and these include linear models and CFD models.

3.1. Linear wind flow models

Linear models are based on a theoretical model of flow over a small hill as developed by Jackson and Hunt (1975) [8]. In this model, wind speed-up induced by a small hill was modeled for neutral atmospheric conditions. They postulate that two regions exist in the lower boundary layer (an inner and outer region) and that the maximum speed-up due to the small hill occurs where the two regions meet near the top of the hill. By defining these two regions and by assuming a logarithmic wind shear profile and neutral atmospheric conditions, a solution to the Navier-Stokes equation was found.

It should be noted that neutral atmospheric conditions represent a very specific situation where the virtual potential temperature is constant with height and there is no convection [14]. In neutral conditions, gravity and buoyancy are equal and opposite so the air has no tendency to rise or fall. This type of condition is often studied in Boundary Layer meteorology since it largely simplifies the equations of motion by eliminating the gravity term. However, while it leads to a simpler solution, it is only applicable to neutral conditions which represents a small fraction of actual conditions (<10%) and occurs during the transition between stable (nighttime) and unstable (daytime) conditions. [14].

Furthermore, since this type of model considers only speed-up over a small hill, its applicability is limited to small hills and can produce wind speed estimates of considerable error (on the order of 5 to 20%), particularly in moderately to highly complex terrain [1–7, 11, 13, 16].

3.2. CFD models

The other main type of wind flow model that is currently used in the wind energy industry is a computational fluid dynamics (CFD) model. In this type of model, a gridded representation of the entire 3-dimensional space of a potential wind farm is created and boundary conditions at the edges of the model are defined. A physical model which can include conservation of momentum, mass or energy is defined and then a solution is sought through an iterative process and the model parameters (pressure, velocity components, turbulent kinetic energy and turbulent dissipation rate) are altered until convergence is achieved.

The physical model is typically represented by the Reynolds-Averaged Navier Stokes (RANS) equation. The RANS equation is the Navier-Stokes conservation of momentum equation but with the terms expressed as a time-averaged component and a fluctuating component which leads to an additional non-linear term named Reynolds stress. In order to close the RANS equation, an additional turbulence model is required and typically a k-epsilon turbulence model is used. [12].

The boundary conditions at the edge of the model describe the wind vertical profile and can be specified using a nested model technique (where the CFD model is "nested" within a larger CFD model) or, as in linear models, the flow can be assumed neutral and logarithmic wind shear profiles are used. By including a temperature profile, stable atmospheric conditions can be modeled in CFD however this can make convergence more difficult. Also, currently, unstable conditions are not modeled in CFD due to its unsteady nature.

3.3. Summary of past validation studies comparing linear and CFD models

Several validation studies have been conducted where linear and CFD models have been compared [1–3, 6, 11, 13, 16] and, in general, there have not been consistent results showing the superiority of either linear or CFD models. Brief summaries of the results of the various studies are given over the next few paragraphs.

In 2003, at the European Wind Energy Conference, a study comparing the application of a linear model (WAsP) and a CFD model (WindSim) at two sites with complex terrain was presented. There were two met towers at each project site and each model was used to cross-predict the wind speeds. For Site 1, the WAsP error was very high at 28.1% and the WindSim error was also large at 19.1%. The error at Site 2 was very similar between the two models with WAsP producing an error of 14.5% and WindSim showing an error of 14.2% [11].

At the European Wind Energy Conference in 2006, a study was presented where WAsP and two CFD models (WindSim and 3DWind) were compared at a site with complex terrain. The site had two 50 m met towers and one 10 m tower. In this comparison, two models of each type were created to represent southerly and northerly wind conditions. For southerly flow, the WAsP and WindSim models showed very similar levels of accuracy with a mean absolute error of 0.11 and 0.10 m/s, respectively, while the 3DWind model showed a higher error of 0.28 m/s. For the model

representing northerly flow, the WAsP model produced a mean absolute error of 0.14 m/s and outperformed both CFD models which both showed a mean error of 0.24 m/s [3].

A CFD validation study in complex terrain was published in 2008 which compared WindSim to WAsP at two sites. Site A was highly complex with 5 met masts while Site B was coastal and had 6 met towers. The overall RMS error of the wind speed estimates for the two models were very similar. For WAsP, an overall RMS error of 3.6% was found while WindSim produced an RMS error of 3.5% [16].

In 2010, a study was presented at the European Wind Energy Conference which compared WAsP and Meteodyn (CFD) at seven test sites. The site complexity ranged from moderate to highly complex terrain and two met masts at each test site were used to cross-predict. The RMS error of the wind speed estimates for the WAsP model was 6.8% while Meteodyn showed an RMS error of 3.1% [13].

In 2011, a paper summarizing the results of the Bolund Experiment was published which was a large group study where 57 different models were compared including large-eddy simulation (LES), CFD-RANS and linear models as well as physical models (i.e. wind-tunnel and water-channel experiments). The blind comparison was based on three months of data measured at nine met towers with a top height of 12 m. The RMS wind speed error of all the modeled results was found to be very high at 17.3%. The CFD-RANS model error was 11.4% while the linear model, WAsP, produced a RMS error of 20.6%. The authors acknowledged that the errors were surprisingly large [2].

A study presented at the Brazil Wind Power Conference in 2012 compared the accuracy of linear and CFD models at four sites with a total of 26 met towers. The RMS error of the wind speed estimates was 0.62 m/s for the linear model (WAsP) and 0.76 m/s for the CFD model (Meteodyn) [1].

In 2012 at the European Wind Energy Conference, the results of a study which compared WAsP and GL-GH's (now DNV-GL) CFD model were presented. In this study, met masts from 13 project sites were used with a total of 74 mets. The RMS error of the wind speed estimates were compared and, for WAsP, the RMS error was 5.2% while the CFD model achieved a better, although still fairly high, RMS error of 3.9% [6].

In the seven studies summarized above, there were some results that showed the WAsP model performing as well as or better than the CFD models and there were also studies which showed the CFD model producing a lower error than WAsP. In general, it is expected that CFD models should produce a more accurate wind flow model however, based on this study review, it was shown that this is not always the case and that the error in CFD models can be substantial.

3.4. Comparison of Linear And CFD Models

The two types of wind flow models most commonly used in the wind industry represent two very different approaches and both have their limitations. With linear models, only the upwind terrain is considered and only the speed-up over a small hill during neutral atmospheric conditions is modeled. Since this represents a small fraction of actual conditions, it is not surprising that large errors can arise. CFD models, on the other hand, consider the entire 3D space and, by modifying the flow parameters, iteratively attempts to find a solution to the RANS equation for each grid cell. Often, neutral atmospheric conditions and logarithmic wind speed profiles are assumed in CFD although stable conditions may be modeled if the temperature profile is specified in the boundary condition. Currently, unstable conditions are not modeled in CFD [18].

Another commonality between linear and CFD models is that the wind flow model is developed based on a single met site and multiple met sites cannot be used simultaneously when creating the model. While some CFD software packages allow for met cross-prediction as a validation check, they do not use more than one met in the model creation. [17, 18].

There are a number of limitations in both linear and CFD models, many of which are avoided in the Continuum model. In Continuum, the only assumption regarding the atmospheric stability or the shape of the wind speed profile is that the average wind conditions are approximately uniform from one met site to another within a project area. Also, in Continuum, all of the met sites are used concurrently when forming the site-calibrated model as opposed to being limited to a single met input as is the case with linear and CFD models. This approach also allows for an estimation of the uncertainty which is represented by the met cross-prediction RMS error.

4. DETAILS OF CONTINUUM MODEL

In the next few sections, the specifics of the Continuum wind flow model are discussed. First, the definition of terrain exposure is given.

4.1. Definition of Terrain Exposure

Terrain exposure (or, simply, exposure) is defined as the weighted average of the elevation differences between a given point and the surrounding terrain within a given radius of investigation weighted by the inverse distance between the two points as shown below in Equation 1.

$$Exposure = \left(\sum_{i=1}^{N} \frac{Z_o - Z_i}{d_{z_o - z_i}}\right) \Bigg/ \left(\sum_{i=1}^{N} \frac{1}{d_{z_o - z_i}}\right)$$

Equation 1. Exposure definition

where Z_0 Elevation at site, m Z_i Elevation at grid point within R,m
$d_{zo\text{-}zi}$ = Distance between points, m R = Radius of investigation, m

The terrain surrounding a site is divided into direction sectors and the exposure is calculated within each sector over a range of radii = 4000, 6000, 8000 and 10,000 m (Figure 1).

4.2. Analytical basis of continuum model

The theory behind Continuum is based on Newton's second law which states that the change in momentum of a moving fluid is equal to the net force acting on that fluid. The Navier-Stokes equation is used to represent Newton's second law and is shown below in Equation 2. The terms on the left-hand side of the equation describe acceleration while the terms on the right-hand side are the force due to the pressure gradient, the shear force and the force of gravity.

$$\rho \left(\frac{\partial v}{\partial t} + v \cdot \nabla v \right) = -\nabla P + \nabla T + F$$

Equation 2. Navier-stokes conservation of momentum

Figure 2 shows a fixed control volume that wind travels through while flowing uphill. The forces acting on this control volume are the force due to the horizontal pressure gradient, P_x, the force due to the vertical pressure gradient, P_z, shear force, τ_{UW}, and the force of gravity, ρg. The acceleration of the control volume is equal to the sum of these forces divided by density as shown in Figure 2 where θ is the slope of the terrain.
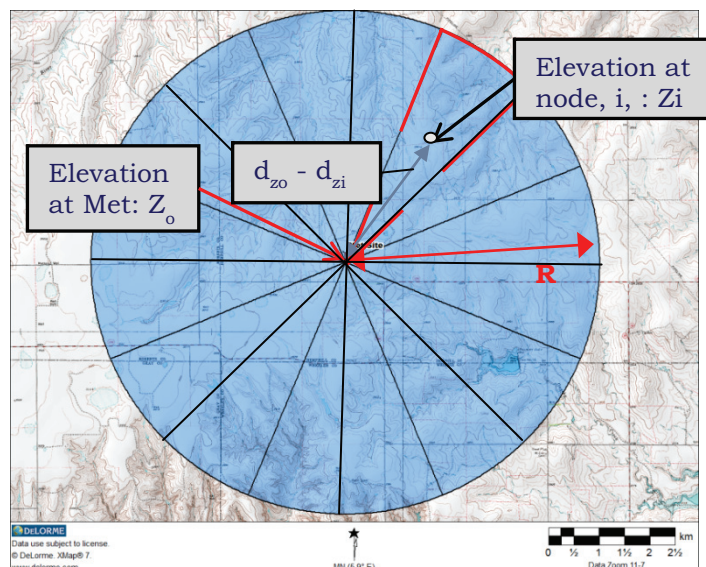
Figure 1. Terrain exposure calculation example

$$\rho a = P_x \cos\theta + P_z \sin\theta - \tau_{UW} - \rho g \sin\theta$$
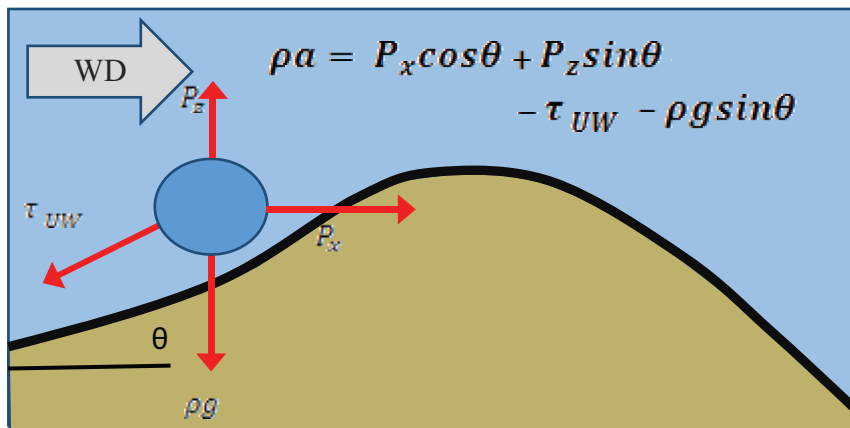
Figure 2. Forces acting on control volume as wind travels uphill

Note that, in Figure 2, the gravity and shear forces are acting against the forces due to the pressure gradient and also note that the gravity and pressure terms are functions of the terrain slope, θ. It then follows that there will be a point at which the sum of the gravity and shear forces are equivalent to the force due to the pressure gradient. This will be discussed in a subsequent section when the induced speed-up over a hill is analyzed.

Next, consider another fixed control volume that wind travels through while flowing downhill as shown in Figure 3. In this scenario, the gravity force and the force due to the horizontal pressure gradient act in the same direction as the flow and in the opposite direction of the shear force and the force due to the vertical pressure gradient. The acceleration of the control volume is equal to the force due to the horizontal pressure gradient plus the force of gravity minus the shear force and force due to the vertical pressure gradient as shown in Figure 3.

The acceleration (or deceleration) of the wind depends on four main factors and those include:

1) Terrain Complexity
   - Slope of terrain, θ, affects the pressure gradient forces and gravity force terms
2) Atmospheric Stability
   - In unstable (turbulent) conditions, the wind is less coupled with terrain and the shear force is lower whereas during stable (laminar) conditions, the wind is more coupled with terrain and this translates to a higher shear force.
3) Air Density
   - The density determines the mass of the air and will therefore affect its momentum.
4) Surface Roughness
   - The surface roughness has a large influence on the shear force which will affect the momentum of the wind.

$$\rho a = P_x \cos\theta - P_z \sin\theta - \tau_{DW} + \rho g \sin\theta$$
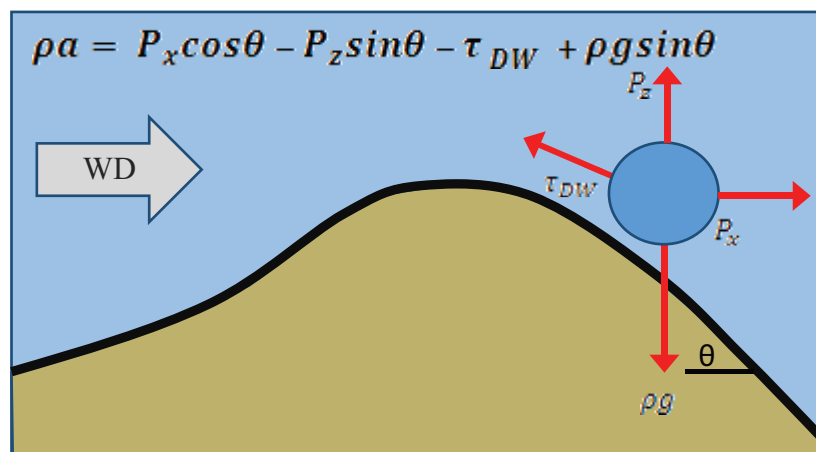
Figure 3. Forces acting on control volume traveling downhill

If it is assumed, for a particular wind direction, that the mean atmospheric stability, air density and surface roughness are uniform across the project area then only variations in the terrain slope will affect the acceleration of the wind. If the wind speed is known at a given location then it can be estimated at another site where there is some difference in the upwind and downwind terrain which would translate into either an increase or decrease in the momentum and therefore the wind speed.

In the next few sections, fixed control volumes with varying UW and DW terrain slopes are considered and the change in the acceleration as the UW or DW terrain changes is examined using the Navier-Stokes conservation of momentum equation.

4.2.1. Control volume with change in downwind (DW) slope: downhill flow

First, let's consider a scenario where the wind speed is known at Site 1 and the upwind (UW) terrain is identical at Site 1 and Site 2 however there is a steeper slope downwind (DW) of Site 2. Simple examples of these two sites are shown in Figures 4 and 5.

The acceleration in the wind speed at the two sites due to the downwind terrain can be written as shown below.

$$Site\ 1: \rho_1 a_1 = P_x \cos\theta_1 - P_z \sin\theta_1 - \tau_1 + \rho g \sin\theta_1$$

$$Site\ 2: \rho_2 a_2 = P_x \cos\theta_2 - P_z \sin\theta_2 - \tau_2 + \rho g \sin\theta_2$$

By subtracting the two equations, the difference in the acceleration from Site 2 to Site 1 can be written as shown below:

$$\rho_2 a_2 - \rho_1 a_1 = (P_x \cos\theta_2 - P_z \sin\theta_2 - \tau_2 + \rho g \sin\theta_2) - (P_x \cos\theta_1 - P_z \sin\theta_1 - \tau_1 + \rho g \sin\theta_1)$$
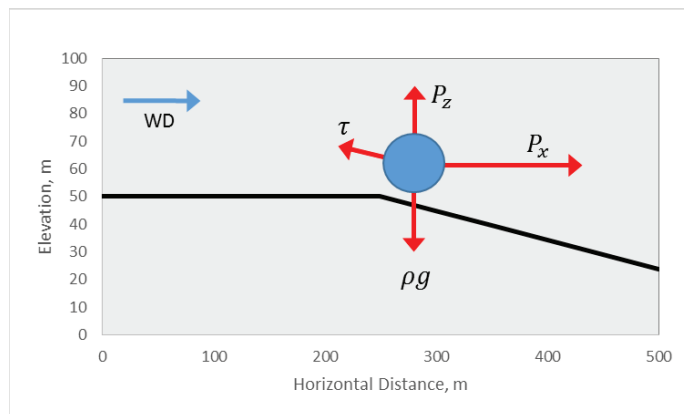
Figure 4. DW example site 1 ($\theta = 8°$)
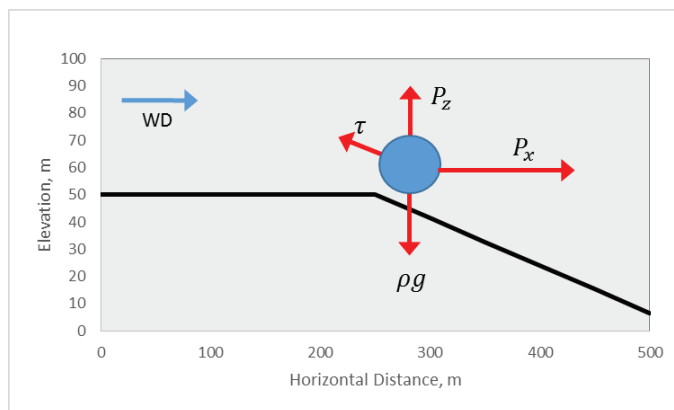
Figure 5. DW example site 2 ($\theta = 10°$)

Next, if the conditions at the two sites are identical in terms of density, surface roughness, atmospheric stability and horizontal and vertical pressure gradient then the difference in acceleration from Site 2 to Site 1 can be estimated as shown below:

$$a_2 - a_1 = \frac{P_x}{\rho}\Delta\cos\theta_{DW} - \frac{P_z}{\rho}\Delta\sin\theta_{DW} + g\Delta\sin\theta_{DW}$$

The slope of the terrain in a typical wind farm can vary from a few fractions of a degree to as high as ~20° and therefore $\Delta\cos\theta$ will be much smaller than $\Delta\sin\theta$ and we can neglect the change in horizontal pressure gradient force term.

$$\Delta\cos\theta \ll \Delta\sin\theta$$

$$a_2 - a_1 = \left(g - \frac{P_z}{\rho}\right)\Delta\sin\theta_{DW}$$

The acceleration term is expanded below and written in terms of velocity and the partial derivatives of velocity with respect to time and Cartesian coordinates.

$$\left(\frac{\partial v_2}{\partial t} + v_2\left(\frac{\partial v_x}{\partial x} + \frac{\partial v_y}{\partial y} + \frac{\partial v_z}{\partial z}\right)\right) - \left(\frac{\partial v_1}{\partial t} + v_1\left(\frac{\partial v_x}{\partial x} + \frac{\partial v_y}{\partial y} + \frac{\partial v_z}{\partial z}\right)\right) = \left(g - \frac{P_z}{\rho}\right)\Delta\sin\theta_{DW}$$

Since we are modeling mean atmospheric conditions, we may assume steady-state conditions $\left(\frac{\partial v_z}{\partial t} = 0\right)$ and two-dimensional flow $\left(\frac{\partial v_y}{\partial y} = 0\right)$ then the equation simplifies to only include the

partial derivatives, $\frac{\partial v_x}{\partial x}$ and $\frac{\partial v_z}{\partial z}$, which describe the rate of change in velocity in the X and Z

directions. Finally, if we assume that the velocity gradients in the X and Z directions are approximately the same at the two sites then the equation simplifies further to Equation 3 shown below:

$$v_2 - v_1 = \frac{\left(g - \dfrac{P_z}{\rho}\right)}{\left(\dfrac{\partial v_x}{\partial x} + \dfrac{\partial v_z}{\partial z}\right)_{DW}}\Delta\sin\theta_{DW}$$

$$\Delta WS = \frac{\left(g - \dfrac{P_z}{\rho}\right)}{\left(\dfrac{\partial v_x}{\partial x} + \dfrac{\partial v_z}{\partial z}\right)_{DW}}\Delta\sin\theta_{DW}$$

Equation 3. Change in velocity due to change in DW slope (DW > 0)

Equation 3 describes the change in wind speed due to changes in the DW slope when the DW slope is positive (terrain slopes down downwind of site) and is a function of the wind speed gradients, $\frac{\partial v_x}{\partial x}$ and $\frac{\partial v_z}{\partial z}$, and the vertical pressure gradient force, $\frac{P_z}{\rho}$.

The first term in the denominator, $\frac{\partial v_x}{\partial x}$, describes the rate of change of the horizontal wind speed along the x-axis. The second term in the denominator, $\frac{\partial v_z}{\partial z}$, represents how the vertical wind speed changes as a function of height. Since vertical wind speeds are typically very small compared to horizontal wind speeds, we can ignore the vertical wind speed gradient and just examine the effect of the horizontal wind speed gradient.

At a site with simple terrain, there will be less wind speed variability than at a more complex one $\left(i.e. \left(\dfrac{\partial v_x}{\partial x} \right)_{SIMPLE} < \left(\dfrac{\partial v_x}{\partial x} \right)_{COMPLEX} \right)$ and if we assume a fixed value for $\dfrac{P_z}{\rho} = 9.6$ m/s^2, we can calculate the change in wind speed due to changes in the DW slope as a function of terrain complexity. These results are plotted in Figure 6 and as $\dfrac{\partial v_x}{\partial x}$ increases, the wind speed becomes less sensitive to changes in the DW slope. Based on this analysis, it is expected that the wind speed at sites with simple terrain will be more sensitive to changes in the DW exposure than at a site with complex terrain.

Next, we can take a look at how the $\dfrac{P_z}{\rho}$ term affects the change in wind speed. This term is related to atmospheric stability and, for neutral atmospheric conditions, it is equal to the gravitational acceleration and, as the atmosphere becomes more stable, $\dfrac{P_z}{\rho}$ decreases. If we assume a horizontal wind speed gradient, $\dfrac{\partial v_x}{\partial x} = 0.0005$ s^{-1} (i.e. 0.5 m/s change over 1000 m), we can examine the change in wind speed due to changes in the DW slope as a function of atmospheric stability as shown in Figure 7. As the atmospheric stability becomes more stable (as $\dfrac{P_z}{\rho}$ decreases), the wind speed becomes more sensitive to changes in the DW slope. This is intuitive since the wind speed becomes more coupled with the terrain as the atmosphere becomes more stable and would therefore react more to changes in the terrain.
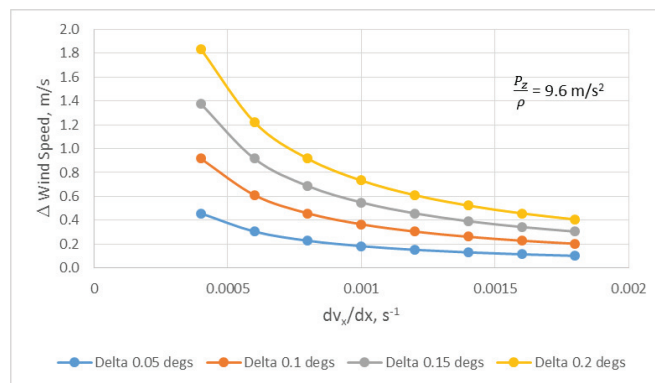
Figure 6. Delta WS vs. horizontal. WS gradient
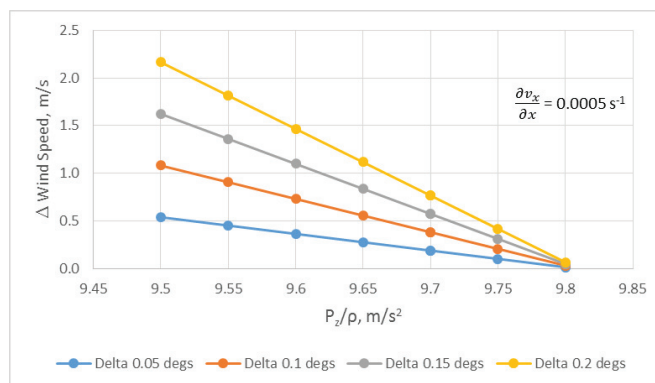
Figure 7. Delta WS vs. vertical pressure gradient force

4.2.2 Control volume with change in upwind (UW) slope: downhill flow

Next, consider a scenario where the wind speed at Site 1 is known, the downwind terrain at Site 1 and Site 2 are identical but the terrain upwind of Site 2 is steeper than the terrain upwind of Site 1. This simplified scenario is depicted in Figures 8 and 9.

The acceleration in the wind speed at the two sites due to the upwind terrain can be written as shown below.

$$Site\,1:\ \rho_1 a_1 = P_x\cos\theta_1 - P_z\sin\theta_1 - \tau_1 + \rho g\sin\theta_1$$

$$Site\,2:\ \rho_2 a_2 = P_x\cos\theta_2 - P_z\sin\theta_2 - \tau_2 + \rho g\sin\theta_2$$

The above equations are the same as in the DW example and if the conditions at the two sites are identical in terms of pressure gradient, surface roughness, atmospheric stability and density then we can subtract the two equations and simplify to find a similar relationship describing the change in wind speed due to a change in the upwind terrain.

$$\Delta WS = \frac{\left(g - \dfrac{P_z}{\rho}\right)}{\left(\dfrac{\partial v_x}{\partial x} + \dfrac{\partial v_z}{\partial z}\right)_{UW}}\,\Delta\sin\theta_{UW}$$

Equation 4. Change in Velocity due to change in UW slope (UW < 0)

Equation 4 describes the change in wind speed due to changes in the UW slope when the UW slope is negative (terrain slopes up upwind of site). If the wind speed at Site 1 is known then the wind speed at Site 2 can be estimated if the wind speed gradient and vertical pressure gradient upwind of the site are known or can be estimated.
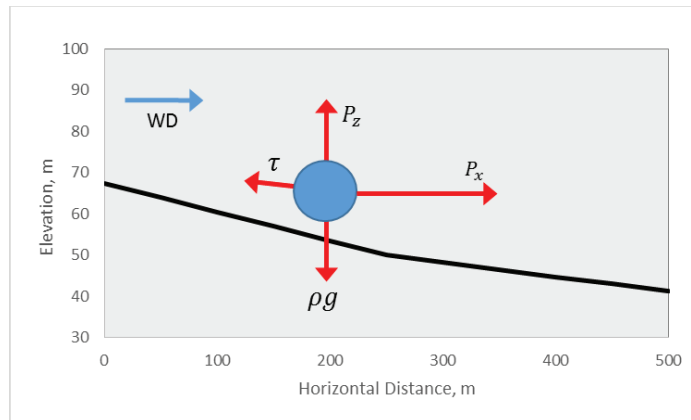
Figure 8. UW example site 1 (θ = −4°)
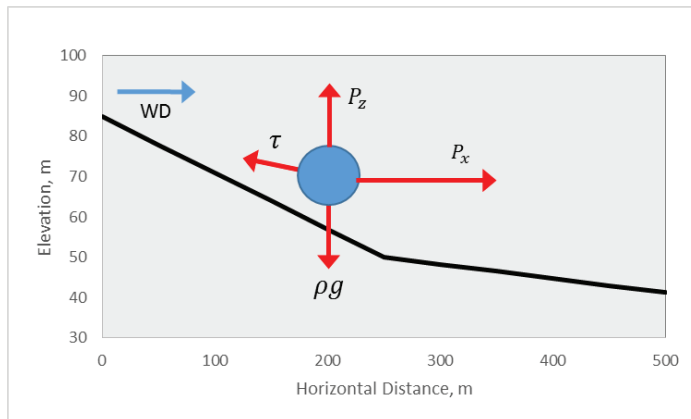
Figure 9. UW example site 2 (θ = −8°)

4.2.3. Control volume with change in upwind (UW) slope: uphill flow

In the previous two examples, the wind was flowing downhill and we examined the effect on the wind speed if the upwind or downwind terrain changed in slope. Next, we consider a control volume that wind travels through as it moves uphill and how changing the upwind terrain slope affects the acceleration.

In this scenario, the sum of the forces acting on the control volume can be written as shown below where the shear force and gravity force act against the force due to the pressure gradient:

$$Site\ 1: \rho_1 a_1 = P_x \cos\theta_1 + P_z \sin\theta_1 - \tau_1 - \rho g \sin\theta_1$$

$$Site\ 2: \rho_2 a_2 = P_x \cos\theta_2 + P_z \sin\theta_2 - \tau_2 - \rho g \sin\theta_2$$

In the last two scenarios, it was assumed that the force due to the pressure gradient was identical at the two sites however, in this situation with the wind flowing uphill, we need to also consider the induced speed-up caused by the hill.

Similar to the previous scenarios, we start by subtracting the two equations and the difference in the acceleration from Site 2 to Site 1 can be written as shown below. Note that the vertical pressure gradient force is written as a function of the terrain slope.

$$\rho_2 a_2 - \rho_1 a_1 = \left(P_x \cos\theta_2 + P_z(\theta_2)\sin\theta_2 - \tau_2 - \rho g \sin\theta_2 \right) - \left(P_x \cos\theta_1 + P_z(\theta_1)\sin\theta_1 - \tau_1 - \rho g \sin\theta_1 \right)$$

$$a_2 - a_1 = \frac{P_x}{\rho}\Delta\cos\theta + \frac{P_z(\theta_2)}{\rho}\sin\theta_2 - \frac{P_z(\theta_1)}{\rho}\sin\theta_1 - g\,\Delta\sin\theta$$

Next, we assume that density, surface roughness, atmospheric stability and horizontal pressure gradient force are identical at the two sites and that $\Delta\cos\theta$ is much smaller than $\Delta\sin\theta$, the equation can be simplified as shown below:

$$a_2 - a_1 = \frac{\left(P_z(\theta_2)\sin\theta_2 - P_z(\theta_1)\sin\theta_1 \right)}{\rho} - g(\sin\theta_2 - \sin\theta_1)$$

And, the acceleration terms are expanded to its partial derivative form as shown below. If we assume that the flow is steady-state and two-dimensional, we can omit the $\frac{\partial v}{\partial t}$ and $\frac{\partial v_y}{\partial y}$ terms.

$$\left(\frac{\partial v_2}{\partial t} + v_2 \left(\frac{\partial v_x}{\partial x} + \frac{\partial v_y}{\partial y} + \frac{\partial v_z}{\partial z} \right) \right) - \left(\frac{\partial v_1}{\partial t} + v_1 \left(\frac{\partial v_x}{\partial x} + \frac{\partial v_y}{\partial y} + \frac{\partial v_z}{\partial z} \right) \right)$$

$$= \frac{(P_Z(\theta_2)\sin\theta_2 - P_Z(\theta_1)\sin\theta_1)}{\rho} - g(\sin\theta_2 - \sin\theta_1)$$

Next, if we assume that the horizontal and vertical wind speed gradients are approximately the same between the two sites then we can group the $\left(\frac{\partial v_x}{\partial x} + \frac{\partial v_z}{\partial z} \right)$ terms and express the difference in wind speed as a function of the change in force due to the pressure gradient and the change in the gravity force term.

$$v_2 - v_1 = \frac{(P_z(\theta_2)\sin\theta_2 - P_z(\theta_1)\sin\theta_1)}{\rho\left(\frac{\partial v_x}{\partial x} + \frac{\partial v_z}{\partial z} \right)_{UW}} - \frac{g}{\left(\frac{\partial v_x}{\partial x} + \frac{\partial v_z}{\partial z} \right)_{UW}}\Delta\sin\theta_{UW}$$

Since the force due to the pressure gradient acts against the gravity and shear forces, there will be situations when the force due to the pressure gradient is larger than the gravity and shear forces and the wind accelerates up the hill and, conversely, there will be times when the gravity and shear forces outweigh the pressure gradient force and the wind decelerates.

The point at which the shear and gravity forces are equal and opposite to the force due to the pressure gradient is defined as the critical upwind exposure, UW_{crit}, where the wind accelerates up the hill if the upwind exposure is less than UW_{crit} and it decelerates if the upwind exposure is greater than UW_{crit}.
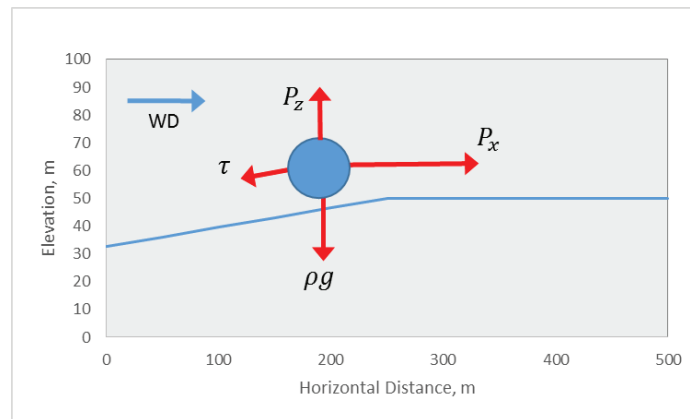
Figure 10. UW example site 3 ($\theta = 4°$)
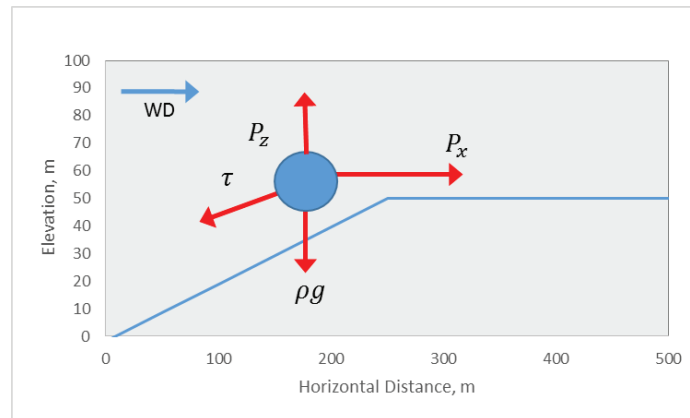
Figure 11. UW example site 4 ($\theta = 8°$)

4.2.4. UW exposure $<$ UW$_{CRIT}$

First, let's consider the situation where the UW exposure is less than the critical UW exposure where the force due to the vertical pressure gradient overcomes the force due to gravity and the wind accelerates over a hill.

The theory of speed-up over a hill has been studied quite thoroughly in boundary layer meteorology and a simplified model to estimate the maximum speed-up as a function of the hill size and shape was presented by Lemelin and Surrey (1988) in their paper "Simple approximations for wind speed-up over hills" [9]. In their paper, they represent a hill in terms of its width and height and present the approximate maximum speed-up as a function of the hill slope as shown in Figure 12 where B is the width of the hill crosswind to the flow and L is the width of the hill parallel to the flow.

As shown, the simple approximation shows a linear increase in the maximum speed-up as the hill slope increases. It also shows that, at a certain hill slope, the maximum wind speed-up reaches a plateau and the additional increase in slope does not translate into a further speed-up of the wind.

Since the speed-up due to the presence of a hill can be approximated as a linear function of the hill slope, it follows that $P_Z(\theta_1) = a*P_Z(\theta_2)$ where a is a constant and we can express the change in wind speed equation as shown below. Then, for small changes in the hill slope, it is assumed that the change in the vertical pressure force is small (i.e. $P_{z1} \approx P_{z2}$) and the change in wind speed approximation is further simplified as shown in Equation 5. For speed-up over a hill, the vertical pressure gradient term is greater than the gravity term and the wind speed increases with an increase in the UW hill slope.
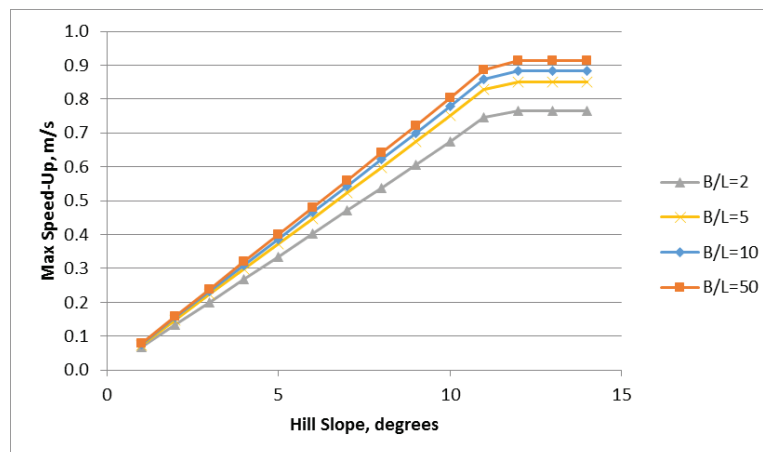
Figure 12. Max speed-up as function of hill slope [9]

$$v_2 - v_1 = \frac{\left(P_{z2}(\sin\theta_2 - \dfrac{P_{z1}}{P_{z2}}\sin\theta_1)\right)}{\rho\left(\dfrac{\partial v_x}{\partial x} + \dfrac{\partial v_z}{\partial z}\right)_{UW}} - \frac{g}{\left(\dfrac{\partial v_x}{\partial x} + \dfrac{\partial v_z}{\partial z}\right)_{UW}}\Delta\sin\theta$$

$$\Delta WS = \frac{\left(\dfrac{P_z}{\rho} - g\right)}{\left(\dfrac{\partial v_x}{\partial x} + \dfrac{\partial v_z}{\partial z}\right)_{UW}}\Delta\sin\theta_{UW} \quad \text{where} \quad \frac{P_z}{\rho} > g$$

Equation 5. Change in velocity due to change in UW slope (0 < UW < UW crit)

4.2.5. UW exposure > UW$_{CRIT}$

If the UW exposure is greater than the critical UW exposure then the gravity force is larger than the vertical pressure gradient force induced by the hill and the wind will decelerate as it travels uphill. If we assume that the vertical pressure gradient force is constant between the two sites then we can express the change in wind speed due to a change in the UW exposure as shown below where the vertical pressure gradient term is less than the gravity term and the wind speed decreases with an increase in the UW hill slope.

$$\Delta WS = \frac{\left(\dfrac{P_z}{\rho} - g\right)}{\left(\dfrac{\partial v_x}{\partial x} + \dfrac{\partial v_z}{\partial z}\right)_{UW}}\Delta\sin\theta_{UW} \quad \text{where} \quad \frac{P_z}{\rho} < g$$

Equation 6. Change in velocity due to change in UW slope (UW > UW crit)

4.3. Summary of derived Δwind speed equations

In the previous sections, the Navier-Stokes conservation of momentum equation was used to examine the effect of changing UW and DW terrain on the acceleration and therefore the velocity of the wind as a function of the UW and DW terrain slope, θ. In Continuum, instead of calculating the average terrain slope, an equivalent measurement (terrain exposure) is used. Recall that terrain exposure is the weighted average elevation difference, Z, between a site and the surrounding terrain within a specified radius of investigation and sin θ can be expressed as the quotient of exposure and the radius of investigation as shown in Equation 7.

$$\sin\theta \equiv \frac{\overline{Z}}{R} = \frac{Exposure}{R}$$

Equation 7

Table 1. Summary of change in wind speed with varying UW and DW terrain

Upwind/Downwind Scenario	ΔWS as function of slope, θ	ΔWS as function of exposure
1) Positive DW Exposure DW> 0	$\Delta WS = \dfrac{\left(g - \dfrac{P_z}{\rho}\right)}{\left(\dfrac{\partial v_x}{\partial x} + \dfrac{\partial v_z}{\partial z}\right)_{DW}} \Delta \sin\theta_{DW}$	$\Delta WS = \dfrac{\left(g - \dfrac{P_z}{\rho}\right)}{\left(\dfrac{\partial v_x}{\partial x} + \dfrac{\partial v_z}{\partial z}\right)_{DW}} \dfrac{\Delta DW}{R}$
2) Negative DW Exposure DW< 0	$\Delta WS = \dfrac{\left(\dfrac{P_z}{\rho} - g\right)}{\left(\dfrac{\partial v_x}{\partial x} + \dfrac{\partial v_z}{\partial z}\right)_{DW}} \Delta \sin\theta_{DW}$	$\Delta WS = \dfrac{\left(\dfrac{P_z}{\rho} - g\right)}{\left(\dfrac{\partial v_x}{\partial x} + \dfrac{\partial v_z}{\partial z}\right)_{DW}} \dfrac{\Delta DW}{R}$
3) Negative UW Exposure UW< 0	$\Delta WS = \dfrac{\left(g - \dfrac{P_z}{\rho}\right)}{\left(\dfrac{\partial v_x}{\partial x} + \dfrac{\partial v_z}{\partial z}\right)_{UW}} \Delta \sin\theta_{UW}$	$\Delta WS = \dfrac{\left(g - \dfrac{P_z}{\rho}\right)}{\left(\dfrac{\partial v_x}{\partial x} + \dfrac{\partial v_z}{\partial z}\right)_{UW}} \dfrac{\Delta UW}{R}$
4) Positive UW Exposure > UW$_{Crit}$ UW> UW$_{crit}$	$\Delta WS = \dfrac{\left(\dfrac{P_z}{\rho} - g\right)}{\left(\dfrac{\partial v_x}{\partial x} + \dfrac{\partial v_z}{\partial z}\right)_{UW}} \Delta \sin\theta_{UW}$ where : $\dfrac{P_z}{\rho} < g$	$\Delta WS = \dfrac{\left(\dfrac{P_z}{\rho} - g\right)}{\left(\dfrac{\partial v_x}{\partial x} + \dfrac{\partial v_z}{\partial z}\right)_{UW}} \dfrac{\Delta UW}{R}$ where : $\dfrac{P_z}{\rho} < g$
5) Positive UW Exposure < UW$_{Crit}$: Induced Speed-up UW$_{crit}$ > UW> 0	$\Delta WS = \dfrac{\left(\dfrac{P_z}{\rho} - g\right)}{\left(\dfrac{\partial v_x}{\partial x} + \dfrac{\partial v_z}{\partial z}\right)_{UW}} \Delta sin\theta_{UW}$ where : $\dfrac{P_z}{\rho} > g$	$\Delta WS = \dfrac{\left(\dfrac{P_z}{\rho} - g\right)}{\left(\dfrac{\partial v_x}{\partial x} + \dfrac{\partial v_z}{\partial z}\right)_{UW}} \dfrac{\Delta UW}{R}$ where : $\dfrac{P_z}{\rho} > g$
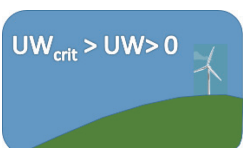
Table 1 summarizes the equations derived from Navier-Stokes for various UW and DW scenarios and describe how the wind speed can be estimated from one site to another by examining changes in the UW and DW terrain both in terms of terrain slope, θ, and terrain exposure.

5. APPLICATION OF CONTINUUM MODEL

In the previous section, equations were derived that describe how the wind speed increases or decreases when the upwind or downwind terrain exposure changes. It was shown that the change in wind speed is a function of the velocity flow field which is related to terrain complexity and it was also shown that the change in wind speed is related to the vertical pressure gradient force which is a function of atmospheric stability.

In this section, we will demonstrate how the theoretical equations can be applied by using coefficients, m_{DW} and m_{UW}, to replace the vertical pressure gradient force, gravity and velocity flow field terms. For each wind direction sector, the coefficients are defined in log-log relationships which are a function of terrain complexity and are defined for downhill and uphill flow as well as induced speed-up over a hill.

5.1. Determination of continuum model coefficients, m_{UW} and m_{DW}

In Table 1, the equations to describe the change in wind speed from one site to another due to changes in terrain exposure are listed and, in each equation, there is a term that describes the vertical pressure gradient force (P_z/ρ), gravity, g, and the wind speed flow field, $\dfrac{\partial v_x}{\partial x} + \dfrac{\partial v_z}{\partial z}$. If we assume, for a particular wind direction, that these forces and velocity flow fields are constant from one site to another then we can define the two coefficients used in Continuum which are the UW coefficient, m_{UW}, and the DW coefficient, m_{DW}. (The equations below represent the coefficients that would be used if the flow is downhill downwind of the site and is uphill upwind of the site.)

$$\Delta WS = \frac{\left(g - \dfrac{P_z}{\rho} \right)}{\left(\dfrac{\partial v_x}{\partial x} + \dfrac{\partial v_z}{\partial z} \right)_{DW}} \frac{\Delta DW}{R} = m_{DW} \Delta DW$$

$$\Delta WS = \frac{\left(\dfrac{P_z}{\rho} - g \right)}{\left(\dfrac{\partial v_x}{\partial x} + \dfrac{\partial v_z}{\partial z} \right)_{UW}} \frac{\Delta UW}{R} = m_{UW} \Delta UW$$

Finally, if we compare two sites where both the UW and DW terrain changes then we can estimate the change in wind speed as shown in Equation 8 below.

$$\Delta WS = m_{UW} \Delta UW + m_{DW} \Delta DW$$

Equation 8. Change in wind speed estimate as function of change in UW and DW terrain exposure

Since the model coefficients, m_{UW} and m_{DW}, are a function of the terrain complexity, a quantitative representation of the terrain complexity is needed which is discussed in the next section.

5.2. Terrain complexity and P10 exposure

In order to apply the Continuum model, a quantitative measure of the terrain complexity was defined and is referred to as the P10 exposure.

The P10 exposure is found by creating a grid around the site (i.e. met, turbine, node or map node) and then calculating the exposure at each node within the gridded area. The calculated exposures are then sorted and the exposure in the top tenth percentile is deemed the P10 exposure and this is a measure of the level of terrain complexity directly surrounding the site.

The idea behind the P10 exposure is that one can represent and quantify the complexity of the surrounding terrain based on how high the exposure is within the surrounding terrain.

The model coefficients are defined as a function of the P10 exposure in log-log relationships as shown in Figure 13.

There are three log-log relationships defined to represent sites with positive or negative UW and DW exposures. One log-log relationship represents sites with downhill flow (i.e. a positive DW exposure or negative UW exposure), another is for sites with uphill flow (i.e. a negative DW exposure or a positive UW exposure (when UW exposure > UW critical)) and a third relationship is used to define the induced speed-up cause by a hill where the UW exposure is less than UW critical. Table 2 below illustrates the various scenarios and the corresponding log-log relationships.
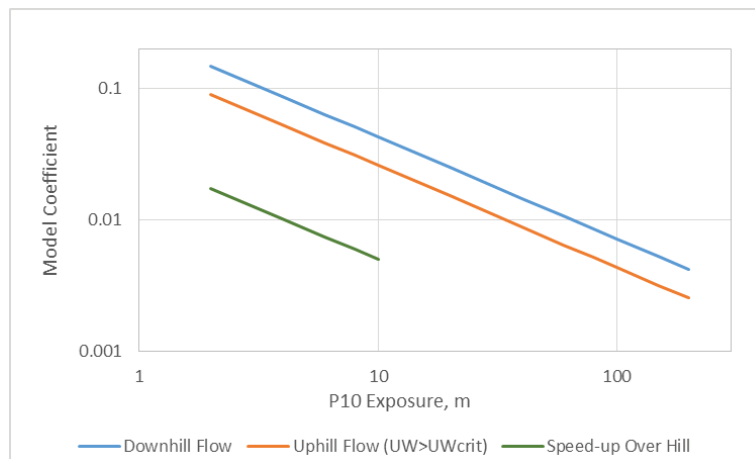
Figure 13. Continuum model coefficients vs. P10 exposure

Table 2. Model coefficients log-log relationships for downhill, uphill and induced speed-up flow
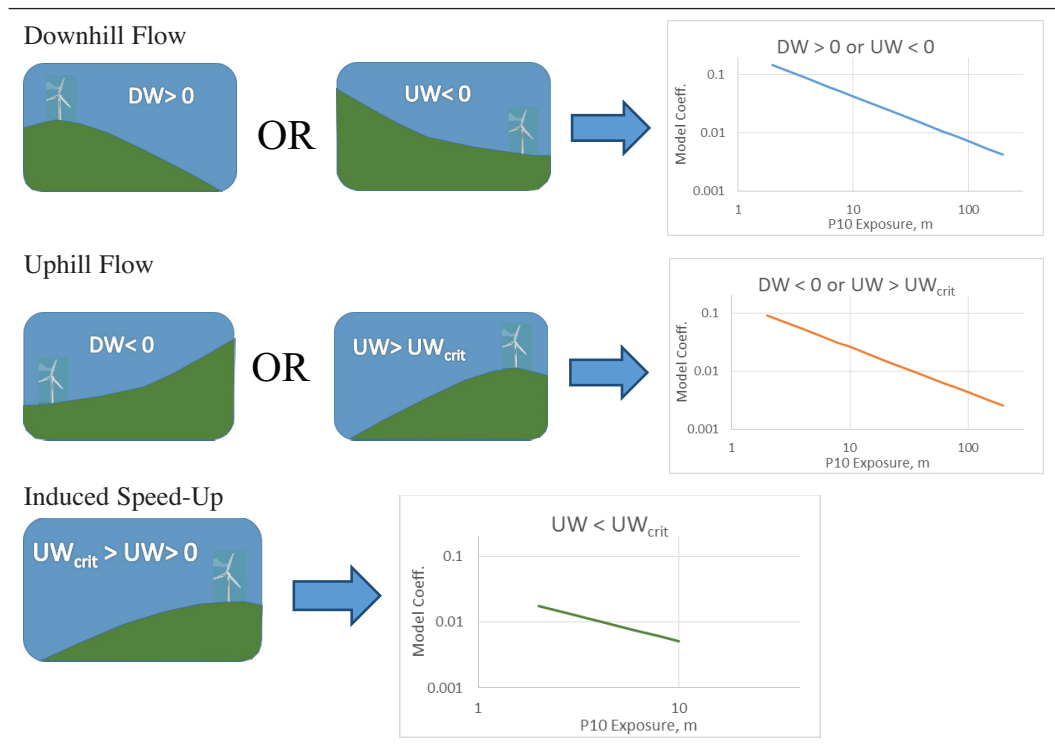
5.3. Stepwise wind speed estimation

Since the terrain complexity can change across a project area, it follows that the model coefficient, which describes the change in wind speed with changes in exposure, should also vary across the project area. For this reason, when estimating the wind speed from one site to another, a path of nodes is created in Continuum that have a gradual change in terrain complexity and elevation. The algorithm selects the path that has the gentlest slope between the two sites and also selects nodes located on high points (as opposed to in a valley, for example).

Once a path between the predictor and target site has been found, the wind speed is calculated along the path of nodes and an estimate at the target site is formed. For each node, the UW and DW coefficients are determined from the three log-log relationships discussed in the previous subsection and are based on the P10 exposure and whether the UW and DW exposures are positive or negative.

5.4 Sectorwise wind speed estimation

One of the assumptions in the Continuum model is that the mean atmospheric stability, surface roughness and density are constant from one site to another and that only changes in the terrain will alter the wind speed. Since, at some sites, the mean atmospheric stability can be quite different as a function of wind direction, the wind speed is estimated from one site to another on a sectorwise basis (Equation 9) where a different set of log-log relationships are defined for each wind direction sector. This allows the model coefficients to be a function of not only terrain complexity but also of mean atmospheric stability.

$$WS_{i,j+1} = WS_{i,j} + m_{UW i,j}(UW_{i,j+1} - UW_{i,j}) + m_{DW i,j}(DW_{i,j+1} - DW_{i,j})$$

where i = 1 to Num. WD sectors
where j = 1 to Num. Nodes in Path

Equation 9. Stepwise and sectorwise wind speed estimate

Once the sectorwise wind speed estimates have been formed at the target site, they are combined by multiplying with the wind rose as measured at the predictor met site to form the overall wind speed estimate (Equation 10).

$$WS = \sum_{i=1}^{WD} WS_{i,N} \times Wind\ Rose\ Freq_i$$

Equation 10. Overall wind speed estimate

5.5. Solving for log-log relationships

For each wind direction sector, three log-log relationships define the model coefficients as a function of the terrain complexity. Since the terrain complexity can change across a project area, Continuum uses a stepwise approach by creating a path of nodes with a gradual change in complexity and the wind speed is estimated from the met site along the path of nodes to the target site. This is done both when conducting the met cross-predictions and when generating the wind speed estimates at the turbine and/or map node sites.

To find the site-calibrated models, Continuum starts with default log-log relationships that have been established after analyzing data from dozens of project sites and the wind speed between each pair of met sites is cross-predicted. (Recall that the exposure is calculated using four different radii of investigation and thus four site-calibrated models are created.) Then, through a self-learning algorithm, the log-log relationships are systematically altered, both in terms of slope and magnitude, and the set of log-log relationships that generate the lowest met cross-prediction RMS error are found. These site-calibrated models are then used to form the wind speed estimates at the turbine sites and map nodes. The met cross-prediction RMS error is used to estimate the uncertainty of the wind speed estimates.

5.6. Forming weighted average wind speed estimate

Once the site-calibrated models have been determined, each met site is used individually to estimate the wind speed at turbine sites or map nodes. A path of nodes with a gradual change in terrain complexity is formed between each met site and the target site and, with four site-calibrated models, four wind speed estimates are formed at the target site for every met site.

Often, the terrain at the target site will be more similar, in terms of terrain complexity, to certain met sites and so the P10 UW and P10 DW exposure is compared between each of the predicting met sites and the target site and a terrain weighting factor for each wind speed estimate, *i*, is calculated as shown in Equation 11.

$$Terrain\ Weight_i = 1 - \left[\frac{|\Delta P10\ DW|_i + |\Delta P10\ UW|_i}{\sum_{n=1}^{N} |\Delta P10\ DW|_n + |\Delta P10\ UW|_n} \right]$$

Equation 11. Terrain weighting factor

Also, for each of the site-calibrated models, the met cross-prediction RMS error is calculated and the model with the lowest RMS error is assigned a higher weight as shown in Equation 12.

$$RMS\ Weight_i = 1 - \frac{0.75 \times (RMS_i - Min\ RMS_i)}{(Max\ RMS - Min\ RMS)}$$

Equation 12. RMS error weighting factor

Finally, using the terrain and RMS weighting factors, the wind speed estimates are combined using a weighted average to form the overall wind speed estimate at the target site.

$$Wind\ Speed\ Weight_i = RMS\ Weight_i \times Terrain\ Weight_i$$

$$Average\ Wind\ Speed\ Estimate = \frac{\sum_{i=1}^{Num\ Ests} WS\ Weight_i \times WS\ Estimate_i}{\sum_{i=1}^{Num\ Ests} WS\ Weight_i}$$

Equation 13. Weighted average wind speed estimate

6. CONTINUUM MODEL: CASE STUDY

To demonstrate the accuracy of the Continuum model, a validation study was conducted at a potential wind farm site in the US with complex terrain where there are eleven met sites situated across the project area. The concurrent data period used in the study was from May 2011 to August 2013 and the data was filtered to only include intervals where valid data was available from all met sites. The ten-minute wind speeds at the top level of each met site (which ranged from 58 to 60 m) were extrapolated to a hub height of 80 m and these extrapolated data sets were used to form the wind speed and wind direction distributions at each site. Using all eleven met sites, a Continuum wind flow model was generated and the wind speed was estimated at each met site location. Additionally, a "Round Robin" analysis was conducted in Continuum where every subset of 8, 9 and 10 met sites was used to create a model and to predict the wind speed at the excluded met sites. The Round Robin analysis provides valuable insight regarding the robustness of the model and the uncertainty of the wind speed estimates. The following section presents the results of the case study.

6.1. Description of wind resource at test site

The prevailing wind direction at the test site is generally from the west with the west-southwest to west-northwest wind direction sectors accounting for more than 60% of the measured wind (Figure 15).

The directional wind speed ratios are shown in Figure 16 where the dotted black line represents a 1:1 wind speed ratio. Figure 16 shows that the highest wind speeds occurred in the southwest wind direction sector.

The mean wind speed at the eleven sites, for the common data period, vary by a fairly large amount with approximately 1 m/s separating the lowest and highest wind speed site.

6.2. Site-calibrated model coefficients

The wind speed and wind direction distributions measured at each met site were entered into Continuum along with 30 m resolution digital elevation data and four site-calibrated models were formed using a radius of investigation of 4000, 6000, 8000, and 10,000 m in the exposure calculation. For each model, paths of nodes with gradually changing terrain complexity were found between each pair of met sites and the wind speeds were cross-predicted using the default model coefficients. Then, through a self-learning algorithm, the downhill and uphill model coefficients were systematically altered until the met cross-prediction error reached a minimum value. The following plots and tables summarize the site-calibrated model coefficients found in Continuum as well as the met cross-prediction error for each model.

Figures 17 to 19 show the site-calibrated model coefficients as a function of wind direction (at a fixed P10 Exposure of 30 m) for the four models. As shown in Figure 17, the west-southwest wind direction sector (240°) yielded the largest downhill coefficient which was approximately 0.04 (for R = 6000 m). The uphill coefficients found through the site-calibration process were lower in
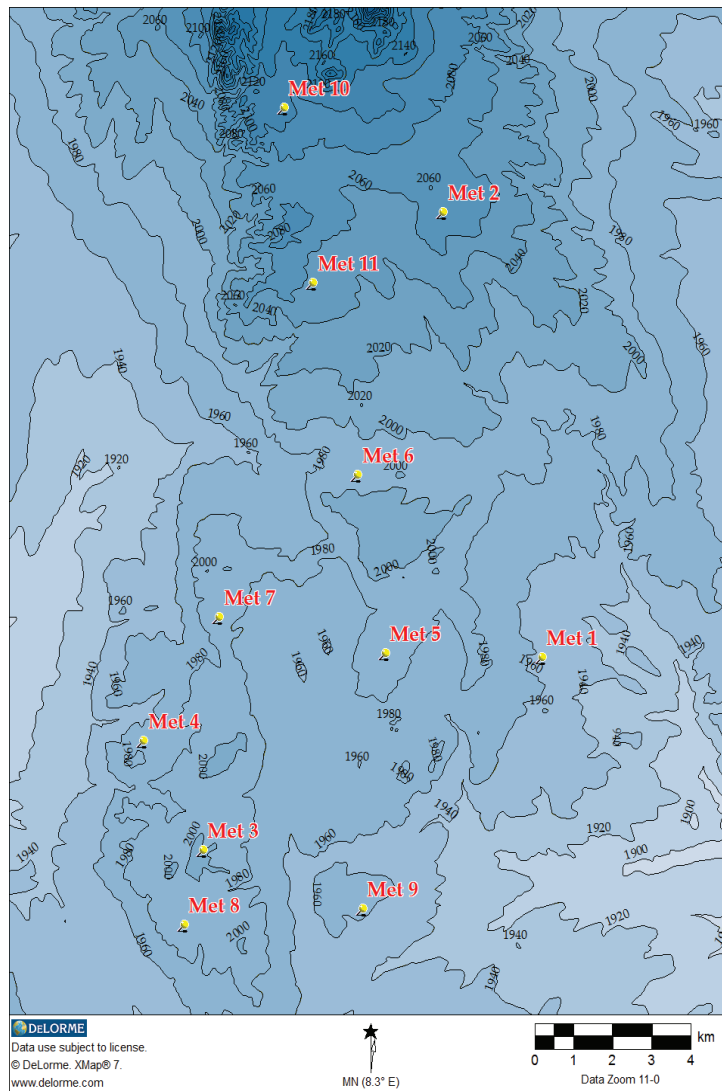
Figure 14. Validation site with 11 met sites
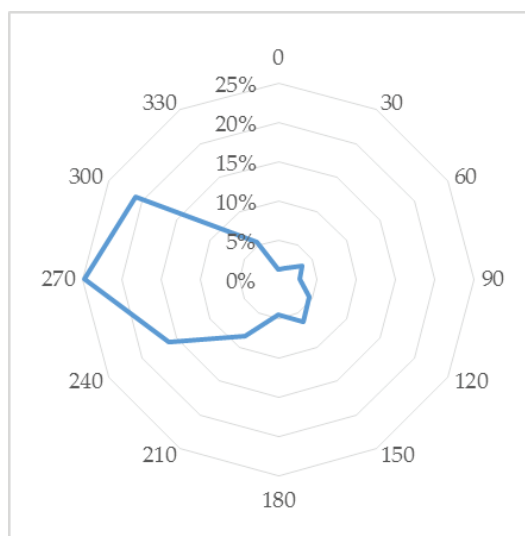
Figure 15. Average wind rose

Table 3. Avg. wind rose

WD, degs	Rose Freq., %
0	1.3%
30	1.7%
60	3.5%
90	2.7%
120	4.5%
150	6.2%
180	4.5%
210	8.4%
240	16.1%
270	24.7%
300	21.0%
330	5.5%
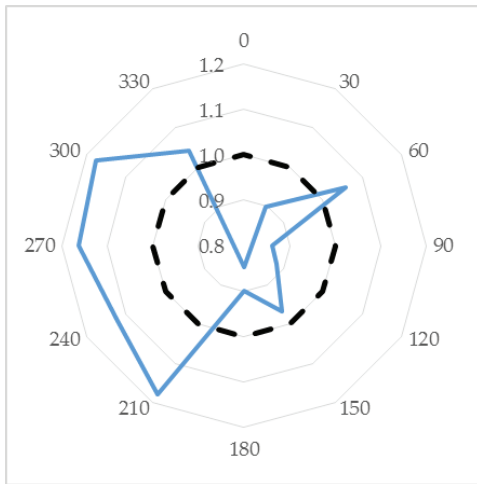
Figure 16. Average directional wind speed ratios

Table 4. Avg. directional WS ratios

WD, degs	Directional WS Ratio
0	0.752
30	0.898
60	1.058
90	0.862
120	0.882
150	0.967
180	0.899
210	1.179
240	1.122
270	1.162
300	1.176
330	1.042
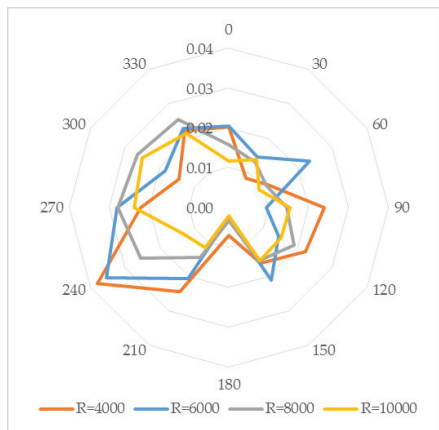
Figure 17. Downhill model coeffs. by WD (P10 expo = 30 m)
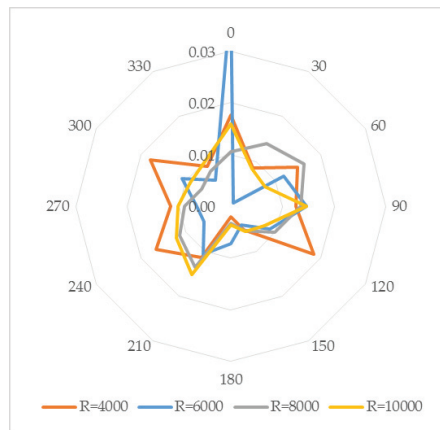
Figure 18. Uphill model coeffs. (UW>UW$_{crit}$) by WD (P10 expo = 30 m)
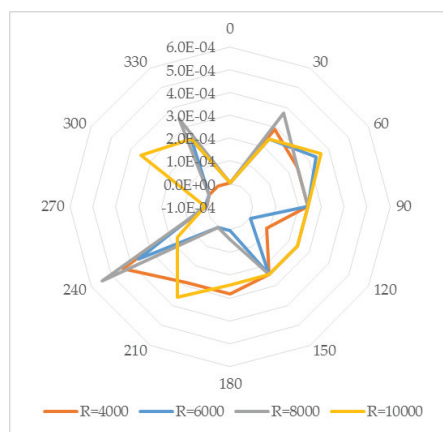
Figure 19. Induced speed-up model coeffs. (UW<UW$_{crit}$) by WD (P10 expo = 30 m)

magnitude than their downhill counterparts. In general, as shown in Figure 18, the uphill coefficients were in the range of 0.01 to 0.02. Figure 19 shows the uphill coefficients when the UW exposure is less than the critical UW exposure and there is induced speed-up over a hill. The magnitude of these coefficients are approximately zero for the wind direction sectors of 270˚ to 0˚ which indicates that there is no induced speed-up due to a hill in these direction sectors. While for

the wind direction sectors of 30° to 240°, the induced speed-up coefficients are quite consistent at a magnitude of approximately 4e-5. These model coefficients are also presented in tables in the Appendix.

The model coefficients for wind direction sectors 240, 270 and 300° are presented as a function of P10 exposure (which is a proxy for terrain complexity) in Figures 20 to 22, for the model which used a radius of 6000 m in the exposure calculation. The site-calibrated model coefficients all showed a dependency on P10 exposure where the coefficients decreased in magnitude as the P10 exposure increased. These coefficients are also presented in tables in the Appendix.

Table 5 shows the RMSE of the met cross-prediction errors for each of the four site-calibrated models. The lowest cross-prediction error was achieved by using a radius of investigation of 6000 m and the RMS error of the met cross-predictions was 1.28%.
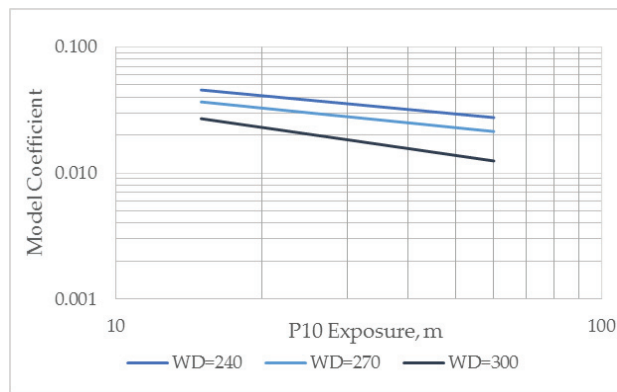
Figure 20. Downhill model coeffs. by P10 expo at WD = 240° to 300° and radius = 6000 m
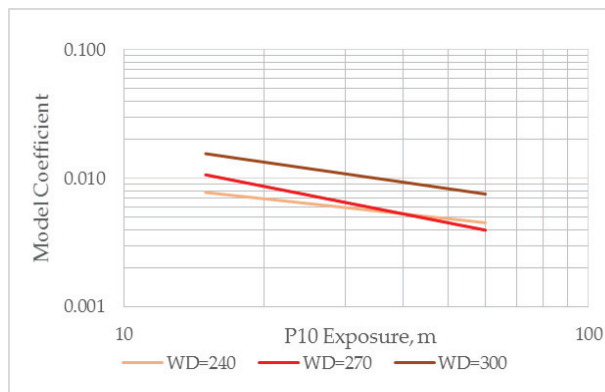
Figure 21. Uphill model coeffs. by P10 expo at WD = 240° to 300° and radius = 6000 m (UW>UW$_{crit}$)
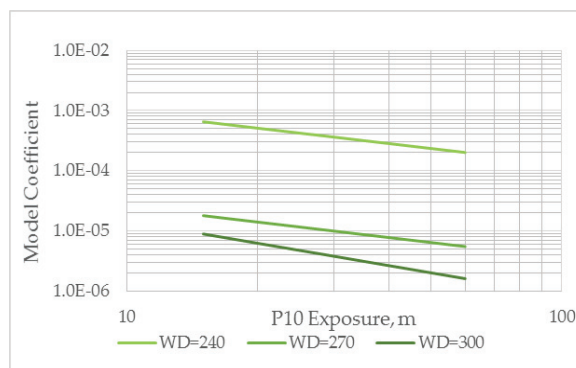
Figure 22. Induced speed-up model coeffs. by P10 expo at WD = 240° to 300° and radius = 6000 m

Table 5. RMS of met cross-prediction error and model weights

Radius, m	RMSE	Weight
4000	2.00%	0.26
6000	1.28%	1.00
8000	1.55%	0.72
10000	2.01%	0.25
Wgt Avg RMS	**1.53%**	

In Continuum, wind speed estimates are generated using each of the four models and the estimates are weighted based on the RMS error of the met cross-prediction. The model that used a radius of 6000 m has the highest weight of 1.0 while the model with the lowest weight of 0.25 used a radius of 10,000 m in the exposure calculation.

6.3. Wind speed ratio estimates at met sites

To test the accuracy of the model, the wind speeds were predicted at the eleven met sites and the results are shown in Tables 6 and 7 and Figures 23 to 25. First, the actual and estimated wind speed ratios are compared in Table 6 and Figures 23 and 24. As shown, the actual and estimated wind

Table 6. Actual and estimated wind speed ratio at met sites

Met Site	WS Ratio Actual	WS Ratio Estimate
Met1	1.022	1.025
Met2	1.060	1.049
Met3	1.003	1.010
Met4	0.964	0.961
Met5	1.029	1.021
Met6	0.951	0.966
Met7	0.987	0.984
Met8	1.009	0.996
Met9	1.011	1.014
Met10	0.976	0.990
Met11	0.989	0.985
Average	**1.0000**	**1.0001**

Table 7. WS estimate error (%) at met sites

Met Site	WS Est. Error, %
Met1	0.38%
Met2	−1.03%
Met3	0.66%
Met4	−0.27%
Met5	−0.85%
Met6	1.61%
Met7	−0.32%
Met8	−1.26%
Met9	0.30%
Met10	1.44%
Met11	−0.35%
RMSE	**0.90%**
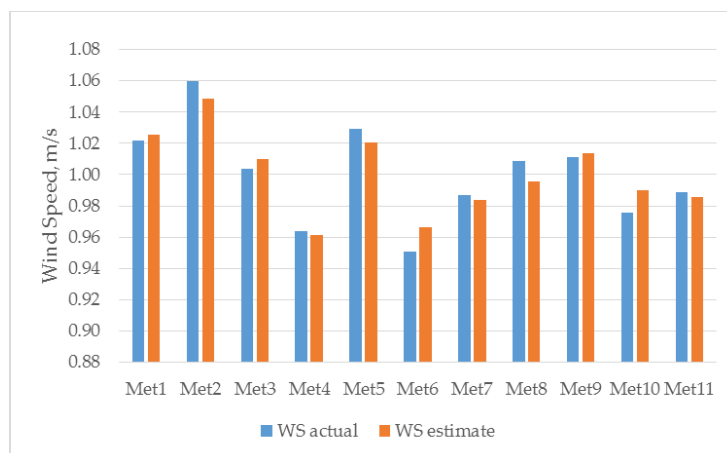
Figure 23. Actual and estimated wind speed ratio at met sites
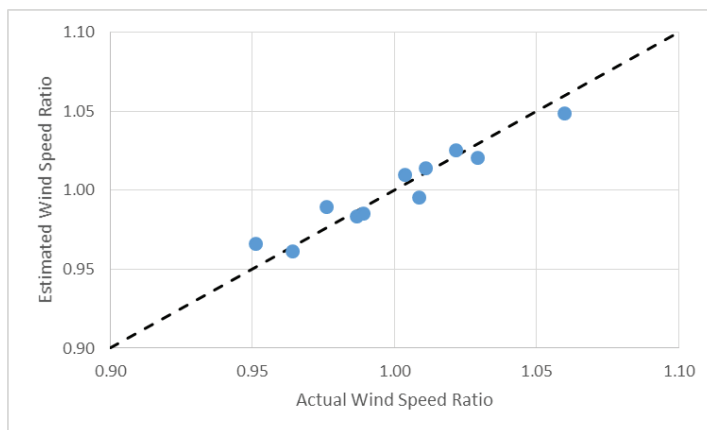
Figure 24. Estimated vs. actual wind speed ratio at met sites
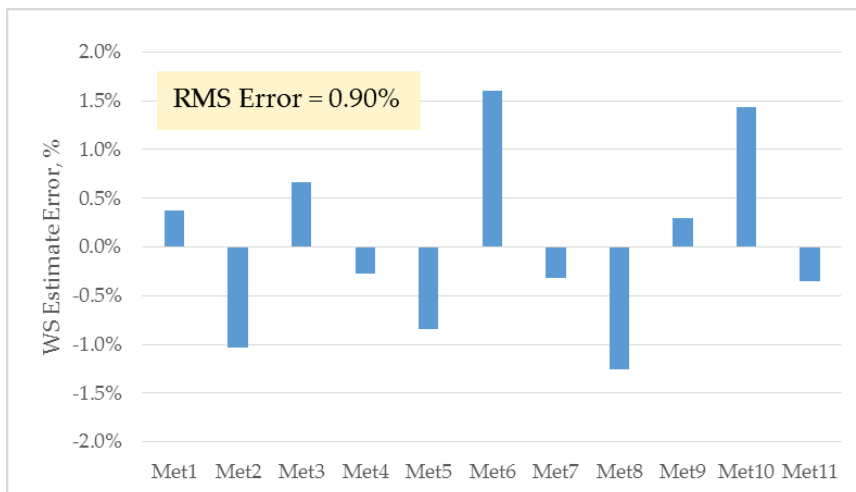
Figure 25. Wind speed estimate error at met sites

speed ratio at each site showed very good agreement. The correlation coefficient, R, between the estimated and actual wind speed ratio was found to be 0.960 and the average estimated wind speed ratio was 1.0001 which indicates that the model did not introduce a bias to the wind speed estimates.

Table 7 and Figure 25 show the wind speed estimate error at each met site. The largest error was measured at Met 6 with an error of 1.61%. Five of the eleven wind speed estimates showed an error of less than 0.50% which is within the uncertainty of the measurement devices. The RMS error of the wind speed estimates was very low at 0.90%.

6.4. Round robin analysis

Since the Continuum model uses all of the met sites simultaneously to create the site-calibrated models, questions might be raised regarding the robustness of the model and about whether the model is over-fitting to the met data. To address these questions and to demonstrate the robustness of the model, in Continuum, a Round Robin analysis may be conducted where every subset of met sites with a size of N-1, N-2 and N-3 met sites (where N = total number of met sites) are used to generate a model which then predicts the wind speed at the excluded met sites.

For each subset size (i.e. N-1, N-2 and N-3 met sites), the RMS error of the wind speed estimates are calculated and this provides valuable insight regarding the quality of the model. The results of the Round Robin analysis for this case study are summarized in the following plots and tables.

With eleven met sites in the case study, the Round Robin analysis created all possible models with 8, 9 and 10 met sites. A total of 11 models were created with a met subset size of 10 mets, 55 models were formed using 9 met sites and 165 models were created for a subset size of 8 met sites. For every model created, the wind speed was calculated at the excluded met sites and the wind speed estimate errors are displayed in Figures 26 to 28. The RMS error is summarized below in Table 8 and showed a consistent RMS error of approximately 1.6% for the three subset sizes.

This Round Robin analysis demonstrates the very good quality of the Continuum models generated at the case study site and provides further confidence in the accuracy of the wind speed estimates.
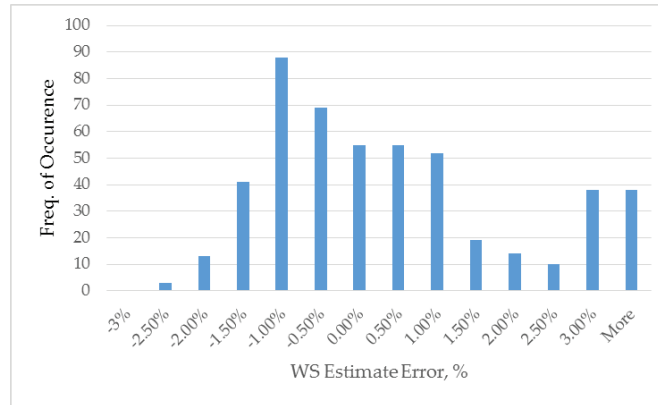
Figure 26. Round robin WS estimate error (%) distribution using subset size = 8 Mets
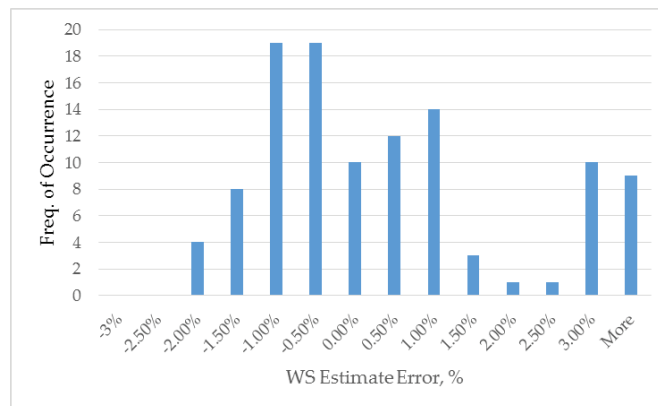
Figure 27. Round robin WS estimate error (%) distribution using subset size = 9 Mets

Figure 28. Round robin WS estimate error (%) distribution using subset size = 10 Mets

**Table 8. RMS error of round robin estimates
using met subset size of 8 to 10 mets**

Number of Mets	RMS Error, %
8	1.61%
9	1.57%
10	1.55%

7. CONCLUSIONS

One of the most important steps in wind resource assessment is accurately defining the wind speed distribution across the project area such that the wind farm can be optimized and will deliver the maximum net energy production. The two types of wind flow models currently used in the wind industry are linear models and CFD models. Linear models are inexpensive, easy-to-use and quick to generate results however there is a strong possibility for large errors particularly in complex terrain. CFD models can generate better quality wind flow models however they require an expert knowledge level, much longer computational time and a significant investment. Furthermore, these types of commercially-available wind flow models only allow for a single met site to be used as an input.

A new wind flow model, Continuum, has been introduced which shares the positive features of both types of models. Continuum is similar to a linear model in that it is simple-to-use, quick to generate results and affordable and yet it has also demonstrated a level of accuracy that is as good as, if not superior, to CFD models. It utilizes all of the met data simultaneously to generate the site-calibrated models and, in essence, Continuum allows the met data to speak for itself. The sensitivity of the wind speed to changes in the UW and DW terrain is a function of terrain complexity and mean atmospheric conditions and the site-calibrated coefficients are determined through a self-learning algorithm that yields the minimum met cross-prediction error. Furthermore, the uncertainty of the generated wind speed and energy estimates are quantified and are based on the met cross-prediction error.

A case study was presented where a site with eleven met towers was modeled in Continuum. The wind speed estimates at the met sites showed excellent agreement with the measured values and the RMS error of the wind speed estimates was 0.90%. Also, a Round Robin analysis was performed in Continuum and demonstrated a high level of robustness where the error of the wind speed estimates at the excluded sites was ~1.6% for all three met subset sizes.

REFERENCES

[1] Beaucage, P. and Brower, M. "Are Advanced Wind Flow Models More Accurate? A Test of Four Models", *Brazil Wind Power Conference* 2012.

[2] Bechman, A., Sorensen, N., Berg, J. and Mann, J. "The Bolund Experiment, Part II: Blind Comparison of Microscale Flow Models", *Boundary-Layer Meteorology,* 2011.

[3] Berge, E., Gravdahl, A., Schelling, J. et al., "Wind in complex terrain. Comparison of WAsP and two CFD-models", *European Wind Energy Conference,* 2006.

[4] Bowen, A. and Mortensen, N. "WAsP prediction errors due to site orography", *Riso National Laboratory,* 2004.

[5] Brower, M., Robinson, N. and Hale, E. "Wind Flow Modeling Uncertainty: Quantification and Application to Monitoring Strategies and Project Design", *AWS Truepower website,* 2008.

[6] Corbett, J., Whiting, R., Bleeg, J et al, "CFD can consistently improve wind speed predictions and reduce uncertainty in complex terrain", *European Wind Energy Conference,* 2012.

[7] Gasset, N., Landry, M. and Gagnon, Y. "A Comparison of Wind Flow Models for Wind Resource Assessment in Wind Energy Applications", *Energies*, 2012.

[8] Jackson, P. and Hunt, J. "Turbulent wind flow over a low hill", *Quarterly Journal of the Royal Meteorological Society*, 1975.

[9] Lemelin, D., Surrey, D. and Davenport, A. "Simple approximations for wind speed-up over hills", *Journal of Wind Eng. Indust. Aerodyn. Vol. 28,* 1988.

[10] Manwell, J., McGowan, J. and Rogers, A. Wind Energy Explained: Theory, Design and Application, *John Wiley & Sons,* 2009.

[11]   Moreno, P., Gravdahi, A. and Romero, M. "Wind Flow over Complex Terrain: Application of Linear and CFD Models", *European Wind Energy Conference*, 2003.

[12]   NASA, "Turbulence Modeling Resource", *turbmodels.larc.nasa.gov*, 2014.

[13]   Pereira, R., Guedes, R. and Santos, S. "Comparing WAsP and CFD wind resource estimates for the "regular" user". *European Wind Energy Conference*, 2010.

[14]   Stull, R. "An Introduction to Boundary Layer Meteorology", *Kluwer Academic Publications*, 1988.

[15]   U.S. Department of Energy Wind Program, "Complex Flow Workshop Report", *DOE website*, 2012.

[16]   Wallbank, T. "WindSim Validation Study: CFD validation in Complex terrain", *www.windsim.com*, 2008.

[17]   WAsP Manual: Wind Analysis and Application Program (WAsP). Vol 2: Users Guide. Risø, National Laboratory, Roskilde, Denmark, ISBN 87-550-178, 1993.

[18]   WindSim documentation. http://windsim.com. 2014.

APPENDIX / TABLES

P10 Expo	30 m			
Radius =	**4000 m**			
WD sect, degs	**Downhill Coeff**	**Uphill Coeff (UW > UWcrit)**	**UWcrit**	**Uphill Speed-up**
0	0.020	0.018	7.5	0.0000
30	0.009	0.009	9.9	0.0003
60	0.011	0.015	16.0	0.0002
90	0.024	0.013	10.0	0.0002
120	0.022	0.019	10.9	0.0001
150	0.016	0.005	15.0	0.0002
180	0.007	0.002	12.9	0.0003
210	0.024	0.011	15.6	0.0003
240	0.038	0.017	12.2	0.0004
270	0.022	0.012	6.6	0.0000
300	0.014	0.018	5.1	0.0000
330	0.022	0.009	7.6	0.0000

Radius =	**6000 m**			
WD sect, degs	**Downhill Coeff**	**Uphill Coeff (UW > UWcrit)**	**UWcrit**	**Uphill Speed-up**
0	0.020	0.040	9.6	0.0000
30	0.014	0.001	15.0	0.0002
60	0.023	0.012	12.4	0.0003
90	0.010	0.015	11.4	0.0002
120	0.014	0.009	7.3	0.0000
150	0.021	0.004	5.5	0.0002
180	0.002	0.007	6.1	0.0000
210	0.021	0.011	7.9	0.0000
240	0.035	0.006	7.1	0.0004
270	0.028	0.007	5.5	0.0000
300	0.018	0.011	5.2	0.0000
330	0.023	0.006	7.5	0.0002

Radius =	8000 m			
WD sect, degs	**Downhill Coeff**	**Uphill Coeff (UW > UWcrit)**	**UWcrit**	**Uphill Speed-up**
0	0.016	0.011	4.9	0.0000
30	0.013	0.014	12.9	0.0004
60	0.011	0.016	10.5	0.0002
90	0.015	0.013	6.1	0.0002
120	0.019	0.010	6.9	0.0002
150	0.015	0.005	8.3	0.0002
180	0.003	0.003	13.6	0.0000
210	0.014	0.014	4.9	0.0000
240	0.025	0.011	5.1	0.0005
270	0.028	0.009	5.4	0.0000
300	0.027	0.006	4.9	0.0000
330	0.025	0.008	7.7	0.0003

Radius =	10000 m			
WD sect, degs	**Downhill Coeff**	**Uphill Coeff (UW > UWcrit)**	**UWcrit**	**Uphill Speed-up**
0	0.012	0.016	5.3	0.0000
30	0.014	0.008	12.5	0.0002
60	0.009	0.008	6.8	0.0004
90	0.015	0.015	6.2	0.0002
120	0.015	0.007	10.5	0.0002
150	0.016	0.006	6.9	0.0002
180	0.002	0.004	7.5	0.0002
210	0.012	0.015	6.1	0.0004
240	0.013	0.012	9.9	0.0002
270	0.024	0.010	6.9	0.0000
300	0.025	0.009	4.9	0.0003
330	0.021	0.010	8.9	0.0002

Radius =	6000 m		
WD =	**240**		
P10 Expo, m	**Downhill**	**Uphill (UW > UWcrit)**	**Uphill Speed-up**
15	0.046	0.008	0.0007
25	0.038	0.006	0.0004
30	0.035	0.006	0.0004
35	0.034	0.006	0.0003
40	0.032	0.005	0.0003
45	0.031	0.005	0.0003
50	0.029	0.005	0.0002
55	0.028	0.005	0.0002
60	0.028	0.005	0.0002

WD =	270		
P10 Expo, m	Downhill	Uphill (UW > UWcrit)	Uphill Speed-up
15	0.037	0.011	0.0000
25	0.030	0.007	0.0000
30	0.028	0.007	0.0000
35	0.026	0.006	0.0000
40	0.025	0.005	0.0000
45	0.024	0.005	0.0000
50	0.023	0.005	0.0000
55	0.022	0.004	0.0000
60	0.021	0.004	0.0000

WD =	300		
P10 Expo, m	Downhill	Uphill (UW > UWcrit)	Uphill Speed-up
15	0.027	0.016	0.0000
25	0.020	0.012	0.0000
30	0.018	0.011	0.0000
35	0.017	0.010	0.0000
40	0.016	0.009	0.0000
45	0.015	0.009	0.0000
50	0.014	0.008	0.0000
55	0.013	0.008	0.0000
60	0.012	0.008	0.0000